Eur. Phys. J. Appl. Phys. (2016) 75: 24716
DOI: 10.1051/epjap/2016150591

THE EUROPEAN PHYSICAL JOURNAL APPLIED PHYSICS

Regular Article

On the study of the mechanical properties of Mo-B-C coatings*

Lukáš Zábranský[1,a], Vilma Buršíková[1], Pavel Souček[1], Petr Vašina[1], and Jiří Buršík[2]

[1]Department of Physical Electronics, Faculty of Science, Masaryk University, Kotlářská 2, 61137 Brno, Czech Republic
[2]Institute of Physics of Materials, Academy of Sciences of the Czech Republic, Žižkova 22, 61662 Brno, Czech Republic

Received: 1 December 2015 / Received in final form: 14 April 2016 / Accepted: 21 April 2016

Abstract. Mo_2BC thin films show a favourable combination of high stiffness, hardness and elastic modulus together with moderate ductility. In this study we focused on the comparison of mechanical properties of Mo-B-C thin films with different structures (nanocrystalline or amorphous). The thin films were deposited on steel, hard metal and silicon substrates using DC magnetron sputtering. The mechanical properties of Mo-B-C films were studied using indentation techniques under both quasistatic and dynamic conditions using a wide range of loads from 50 μN up to 1 N. The results showed that even amorphous Mo-B-C thin films had high hardness of 19.5 ± 0.5 GPa and elastic modulus of 276 ± 5 GPa. Their hardness is comparable with the common amorphous diamond-like carbon coatings. Moreover, their fracture toughness is significantly higher. The results of mechanical tests were correlated with microstructure observations carried out using scanning and transmission electron microscopy. The images of the deformed area under the residual indentation imprints showed no cracking even after high loads or after indentation with sharp cube corner indenter.

1 Introduction

Hard and wear resistant coatings employed for protection of cutting tools exhibit high hardness and stiffness which are often accompanied with brittle deformation behaviour. Cracking can consequently lead to coating failure and thus reduces the lifetime of the coated tool. It is therefore favourable to combine high stiffness, hardness and elastic modulus with moderate ductility to reduce crack initiation and propagation. There are two criteria which are generally used for determination if the material is brittle or ductile. Pugh [1] showed that if the ratio of bulk modulus to shear modulus B/G is greater than 1.75, the material exhibits ductile metal-like behaviour. Otherwise, the material is considered brittle. Pettifor [2] showed that the value of the Cauchy pressure can also give information about ductility. Cauchy pressure is determined as the difference between elastic constants C_{12}–C_{44}. If it is negative, material is brittle. Positive Cauchy pressure, on the other hand, implies ductile behaviour.

Based on previous ab initio calculations [3,4], the material Mo_2BC has a desired combination of high Young modulus of 470 GPa and moderate ductility with $B/G = 1.74$ and Cauchy pressure of +43 GPa [3]. The Mo_2BC material belongs to nanolaminates exhibiting similar structure as the well known MAX phases [5,6] (M = transition metal, A is a group A element and X is either boron or carbon). Emmerlich et al. [3] prepared thin films of this material on Al_2O_3 substrate (temperature of 900 °C) using DC magnetron sputtering. The surface roughness measured by scanning probe microscope (SPM) was in the order of nm. The chemical composition was determined by Rutheford backscattering spectroscopy (RBS) and elastic recoil detection analysis (ERDA) as 49 at.% Mo, 27 at.% B and 24 at.% C. The Young modulus of 460 ± 21 GPa and hardness of 29 ± 2 GPa were measured by nanoindentation using the load of 5 mN. 80% of the deformation energy was dissipated during plastic deformation. The maximum depth was 290 nm and the pile-up around residual imprints was 20–50 nm high.

Bolvardi et al. [4] simulated properties of M_2BC phases for M = Ti, V, Zr, Nb, Mo, Hf, Ta, W. The highest density of valence electrons and the highest Young modulus were obtained for M = Mo, W or Ta. In another paper Bolvardi et al. [7] managed to prepare crystalline Mo_2BC thin films using high power pulsed magnetron sputtering (HPPMS) with synthesis temperature of 380 °C while the synthesis temperature in case of standard DC magnetron sputtering was found to be 550 °C. Because the crystallization temperature of as deposited amorphous Mo_2BC powder was measured by differential scanning calorimetry as 820 °C, the ion bombardment induced surface diffusion was considered as the main reason for the lower synthesis temperature.

[a] e-mail: zerafel@mail.muni.cz

* Contribution to the topical issue "6th Central European Symposium on Plasma Chemistry (CESPC-6)", edited by Nicolas Gherardi, Ester Marotta and Cristina Paradisi

Table 1. Summarized deposition conditions, "(p)" means that the power was pulsed with frequency 350 kHz and duty cycle 65%. Otherwise, the power was DC.

Sample name	Power on a target [W]				Bias voltage [V]	Deposition time [min]	Temperature [°C]
	B_4C	C	Mo	Mo_2BC			
A1	–	–	–	250 (p)	–	180	No heating
A2	–	–	–	250 (p)	−200	420	No heating
C1	128	278 (p)	91	–	−200	480	350
C2	128	250 (p)	110	–	–	480	500
C3	104	281	84	–	−200	300	No heating

In this work the mechanical properties of nanocrystalline (partially crystallized) and amorphous Mo-B-C thin films were compared. The films were deposited on steel, hard metal and silicon substrates using DC magnetron sputtering. Even the amorphous films showed relatively high hardness and elastic modulus which could be compared to common diamond-like carbon (DLC) material discussed see for example in [8]. The study of residual indentation imprints for the loads up to 1 N revealed that no cracking occurred even after the indentation depth exceeded the film thickness. This implies very good fracture toughness of the studied material.

2 Experimental

Several samples were prepared using magnetron sputtering of (i) a single Mo_2BC target (Mo-B-C coatings marked with A) or (ii) three targets: B_4C, C and Mo (Mo-B-C coatings marked with C) in order to better control the stoichiometry. The hard-metal (cemented tungsten carbide, WC-Co), high speed steel (HSS) and silicon substrates were ultrasonically cleaned in a degreasing agent and then placed in the chamber using load-lock system. Prior to the deposition process all substrates were cleaned in argon plasma for 20 min. The deposition pressure was 0.3 Pa. The deposition conditions are summarized in Table 1. In case of HSS substrate an 80 nm thick molybdenum interlayer was deposited prior the deposition of Mo-B-C film. The temperature on the substrate holder for sample C1 and C2 was 350 °C and 500 °C, respectively. The RF bias −200 V was used in some cases (see Tab. 1). The thickness of all coatings was in the range from 1 to 2 μm.

The hardness and elastic modulus were measured and evaluated by depth sensing nanoindentation technique performed on a Hysitron TI950 Triboindenter equipped with a Berkovich tip. The tip diameter was less than 50 nm. The nanoscale measuring head with resolution of 1 nN and load noise floor less than 30 nN was used for this study. Several testing modes were used in the range of indentation loads from 0.1 to 10 mN, namely quasistatic nanoindentation test, quasistatic nanoindentation with several unloading segments and nanodynamic mechanical analysis (nanoDMA) in the range from 0.1 to 300 Hz. The quasistatic indentation tests were carried out in load controlled regime using constant loading rate of 0.2 mN/s. Both the partial unload regime and the nanodynamical analysis were carried out in constant strain rate regime. The pre-load of 2 μN was set to ensure good contact between the tip and the surface. The indenter tip calibration was carried out for low loads (indentation depths <100 nm). The depth profiles of the hardness and elastic modulus were carried out in the load range from 0.25 to 10 mN. The standard procedure proposed by Oliver and Pharr [9] was used for the evaluation of the hardness and elastic modulus.

Further, the cube-corner indenter with tip radius of about 30 nm and with centerline-to-face angle of 34.3° was used to study the prepared films. This very sharp indenter is commonly used to produce well-defined cracks around indentation prints in order to estimate the fracture toughness of thin films at very small scales.

Moreover, several quasistatic indentation test were performed using a Fisherscope H100 instrumented indentation tester at maximum load of 1 N in order to study the differential hardness [10,11] and the fracture resistance of the coating/substrate system. Berkovich indenter with tip radius of 200 nm was used for these tests. The load increase was controlled according to function $L = Ct^2$, where L is the load, t is the time and $C = 2.5$ mNs^{-2}. The differential hardness was calculated as the derivative of the indentation load according to the contact area. The differential hardness dependence on the indentation depth is used to visualize the defect creation in the tested materials.

X-ray diffraction was used in order to determine whether the material is crystalline, nanocrystalline or amorphous. Measurements of X-ray diffraction were performed on Rigaku Smartlab X-ray diffractometer with a fixed angle of incidence. The grazing incidence configuration was used. The details of microstructure in the vicinity of indentation prints made with indentation load of 1 N were studied by means of electron microscopy. Thin lamellas were prepared using a focused ion beam (FIB) technique in a scanning electron microscope (SEM) LYRA 3 XMU FEG/SEM×FIB by Tescan. The lamellas were further studied using transmission electron microscopes (TEM) Philips CM12 STEM (thermoemission source, accelerating voltage 120 kV) and JEOL JEM-2100F (FEG, accelerating voltage 200 kV). The surface morphology was analyzed by an atomic force microscope Ntegra Prima NT-MDT in a semi-contact mode. The area of 10×10 μm was studied using a 20 μm/s scan rate.

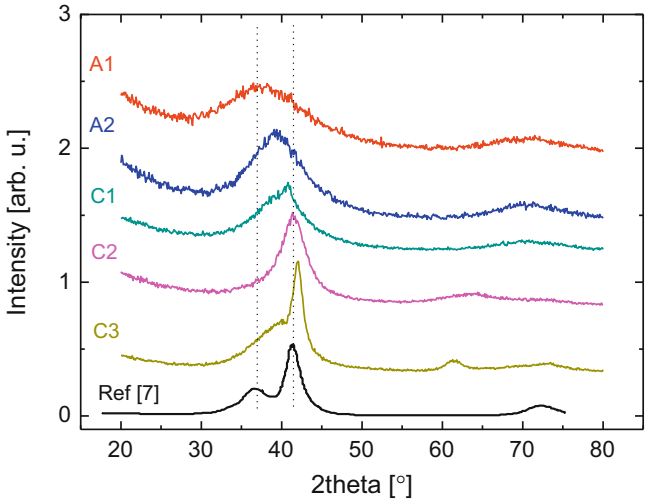

Fig. 1. The diffraction patterns of five films compared with Ref. [7].

3 Results and discussion

The microstructure of Mo-B-C films deposited on WC substrates was studied by both, X-ray diffraction and TEM. The diffractograms presented in Figure 1 are compared with results obtained by Bolvardi et al. [7] on Mo_2BC film prepared using high power pulsed magnetron sputtering (HPPMS) at substrate temperature of 480 °C. According to [7], the appearance of two distinctive peaks at around 36° and 42° indicates the crystalline character of the films. The peak around 42° becomes stronger for films with increasing crystalline content in Mo-B-C films and it originates mainly from Mo_2BC (1 1 1) signal, however, it may be overlapped by Mo_2BC (0 8 0). The wide band at around 36° is an overlap of several peaks instead of signal arisen from amorphous Mo-B-C matrix. The diffractogram presented at the top in Figure 1 shows only a wide band at around 36° suggesting the formation of an amorphous structure for coating marked as A1. The diffractogram of sample A2 contains one wide band situated between 36° and 42° which may represent some transition between amorphous and nanocrystalline state. The combined Rutheford backscattering spectroscopy (RBS) and the elastic recoil detection analysis (ERDA) showed that all coatings prepared using sputtering of one Mo_2BC target were far from the stoichiometric composition (the atomic percentage of Mo differed from the stoichiometric one by more than 10%). The sample group C was prepared using sputtering of three targets (see Tab. 1). What dominates in the diffractograms of this group is a more or less asymmetric broad peak between 36° and 42°, which arises from an overlap of several peaks including an amorphous band. This peak suggests partially crystalline (nanocomposite) structure for samples C1, C2 and C3, which was also proven by TEM study. Moreover, the diffractogram of sample C3 exhibits a significant increase in Mo_2BC (1 1 1) signal indicating substantial increase in volume fraction of Mo_2BC crystallites. The sputtering of three targets (see Tab. 1) enabled a better control of the film stoichiometry, therefore the C samples prepared using this method exhibit a partial crystallinity even without any sample heating as it is proven in case of sample C3.

The microstructure of amorphous coating A1 deposited on hard metal substrate is depicted on TEM micrographs in Figure 2. A wavy coating/substrate interface and heavily deformed grains of hard metal, but no cracks or marks of adhesive failure are observed (Fig. 2a). Both the high resolution image and the selected area diffraction (SAD) pattern (Fig. 2b) confirm the amorphous character of the deposited layer.

The microstructure of nanocrystalline coating C3 deposited on an HSS substrate is shown in Figure 3. The thin lamella prepared by FIB in SEM (Fig. 3a) represents the central vertical section of an indentation print. Global TEM view (Fig. 3b) shows the deformed structure free of any cracks and interfacial failures. A detailed view (Fig. 3c and a high resolution image in Fig. 3d) shows nanosized columnar grains with amorphous material in between.

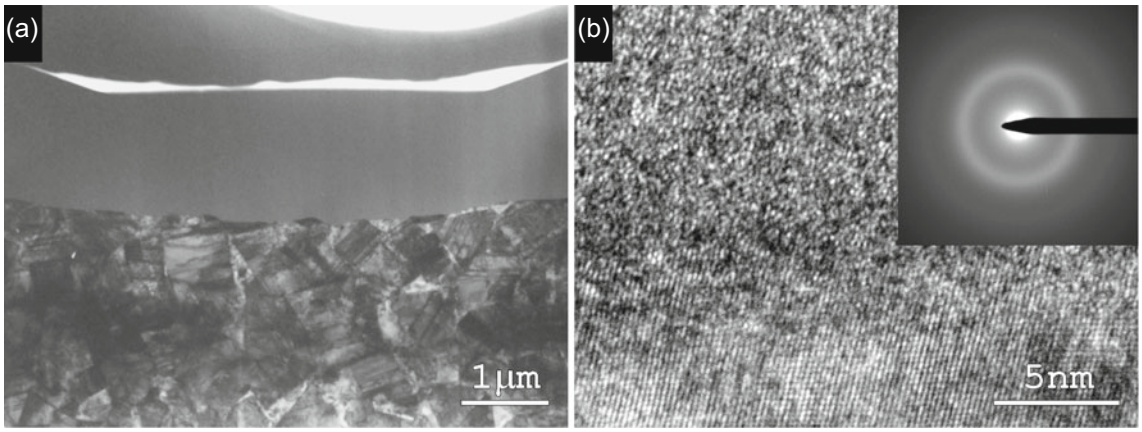

Fig. 2. The microstructure of amorphous coating A1 deposited on hard metal substrate. A global TEM view of the volume under indentation print (a) and a high resolution TEM micrograph of WC grain at the bottom part and an amorphous layer above with SAD pattern (b).

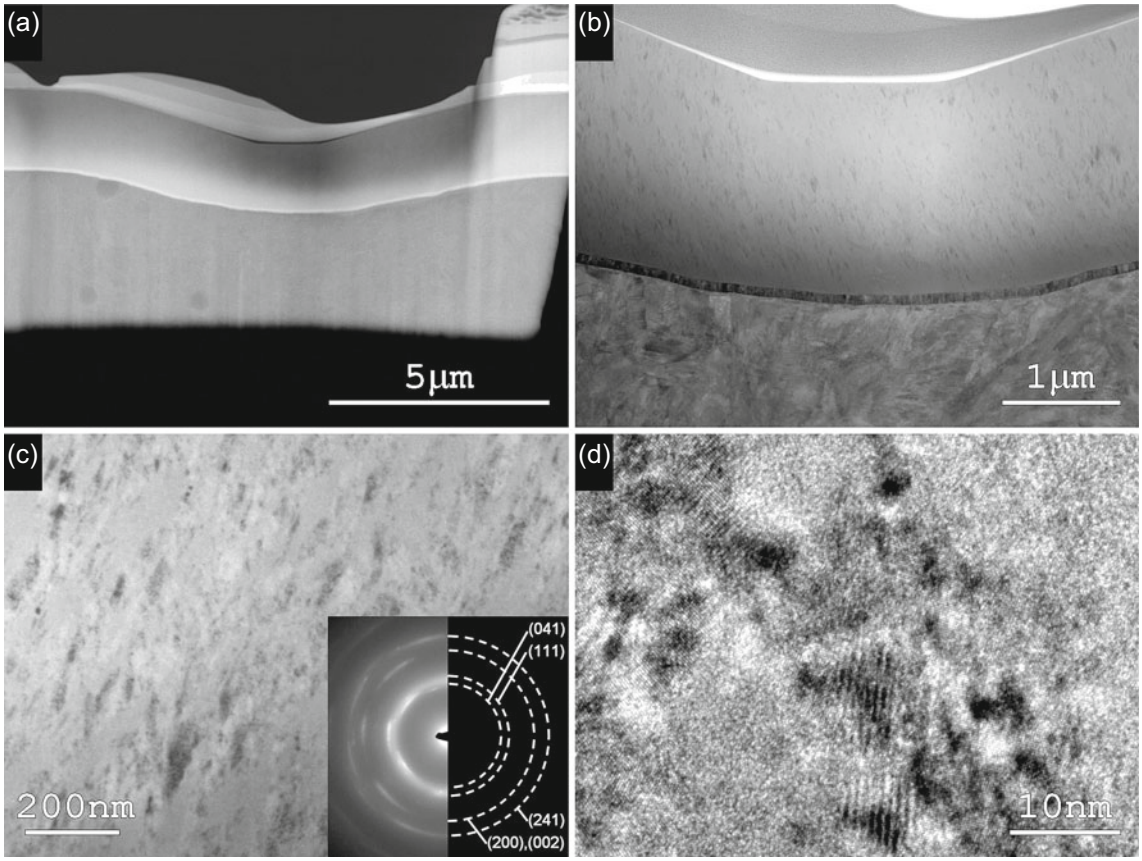

Fig. 3. The microstructure of the coating C3 deposited on an HSS substrate. The final stage of lamella preparation using a FIB in SEM, signal of backscattered electrons (a), a global TEM view of the volume under indentation print (b), a detail of the columnar microstructure with inserted SAD pattern (c) and a high resolution TEM micrograph (d).

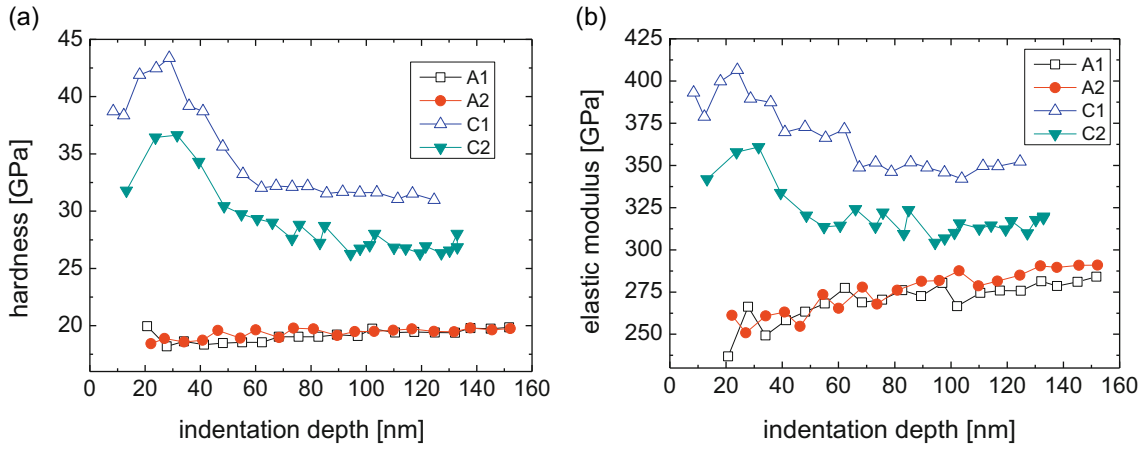

Fig. 4. The evolution of (a) hardness and (b) elastic modulus as functions of maximum indentation depth. The behaviour of these parameters differed with depth for amorphous and nanocrystalline coatings due to different intrinsic stress and microstructure.

The SAD pattern in Figure 3c confirms the Mo_2BC orthorhombic lattice (ICSD entry no. 043318, [12]). The diffraction patterns are assigned to (0 4 1), (1 1 1), (2 0 0), (0 0 2) and (2 4 1) planes of the Mo_2BC structure. The structure of SAD pattern indicates the presence of preferential orientation for Mo_2BC nanocrystallites.

The evolution of hardness and elastic modulus for all four samples deposited on hardmetal substrates is presented in Figure 4 as a function of maximum indentation depth. The error of these measurements was always <10%. Because the thickness of the coatings was larger than 1.0 μm, the values of hardness and elastic modulus taken from depths $<$ 100 nm should not be influenced by the substrate. However, in case of partially crystalline coatings C1 and C2 there is a significant increase in the hardness as well as elastic modulus at

Table 2. Calculated hardness H, elastic modulus E and their ratios H/E and H^3/E^2 for all five films.

Sample name	H [GPa]	E [GPa]	H/E	H^3/E^2 [GPa]
A1	19.4 ± 0.5	272 ± 5	0.071	0.099
A2	19.6 ± 0.5	280 ± 5	0.070	0.096
C1	27.2 ± 0.9	313 ± 11	0.087	0.205
C2	31.6 ± 0.8	345 ± 9	0.091	0.259
C3	20.6 ± 2.0	275 ± 16	0.075	0.116

the sample surface. The tip was carefully calibrated in the region of low indentation depths (between 20 nm and 100 nm) on certificated fused silica standard, therefore this increase does not arise from artefacts connected with imperfect indenter tip. The increased surface hardness compared to the bulk part of samples C1 and C2 is probably caused by internal stress evolution during the growth and due to nonhomogeneous microstucture through depth profile of the nanocomposite films. For comparison of the material parameters in Table 2, the values from greater depths were taken. The optimum depth for bulk hardness and elastic modulus evaluation was considered for the maximum indentation depth of 100 nm. This indentation depth is less than 10% of the film thickness.

The measured and calculated hardness H, elastic modulus E and their ratios H/E (measure of toughness) and H^3/E^2 (resilience) are presented in Table 2. The highest hardness of 31.6 ± 0.8 GPa was found for nanocrystalline sample C1, the highest elastic modulus was 345 ± 9 GPa for the same sample. The average hardness for amorphous samples was 19.5 ± 0.5 GPa and elastic modulus 276 ± 5 GPa.

The cube corner indenter was used and several imprints with maximum load of 10 mN were performed in order to study the crack resistance. The load-displacement curves revealed no sudden pop-in events in any of the samples. There was no cracking induced by the indentation up to 10 mN which indicated very good crack resistance [3]. In Figure 5a, there is a typical load-displacement curve, here for sample C1. Several measurements of differential hardness for sample C1 are plotted in Figure 5b. Differential hardness is calculated numerically from the loading curves for the maximum load of 1 N and it describes the instantaneous resistance of the material to deformation. It is important to state that the initial part (about first 200 nm) of the differential hardness curves strongly depends on the local structure, and is therefore very sensitive to any inhomogeneities such as grain boundaries. No large sudden drops in evolution of differential hardness also implied no cracking events, even for the load of 1 N. Here the maximum indentation depth exceeded the coating thickness and indentation induced plastic

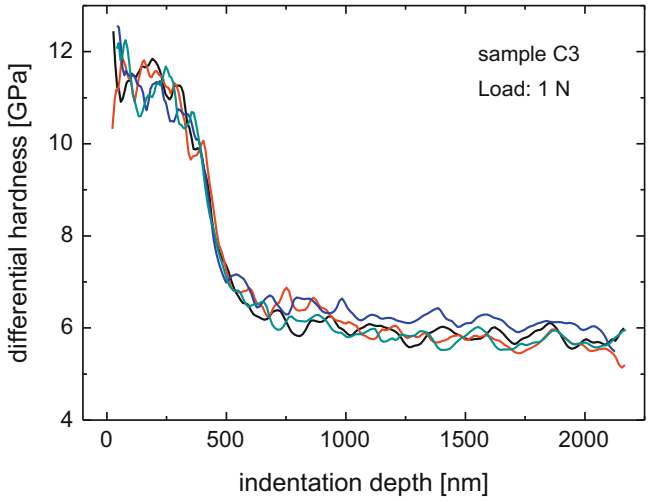

Fig. 6. The differential hardness dependence on the indentation depth for sample C3. The sudden differential hardness decrease from indentation depth of about 0.25 μm is caused by the expansion of the deformation zone into the substrate. The indentation response of the studied sample is fully controlled by plastic deformation of the HSS substrate from indentation depths of about 0.5 μm. Although the maximum indentation depth exceeded the coating thickness, indentation induced cracking was not observed.

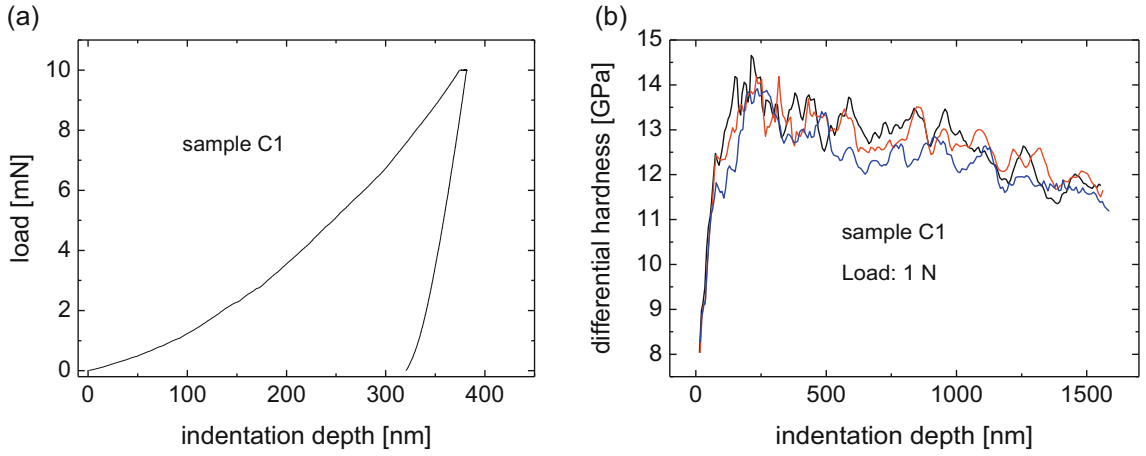

Fig. 5. (a) The example of load/displacement curve for maximum load of 10 mN performed using a cube corner indenter, and (b) three curves of differential hardness dependence on the indentation depth. No pop-in events in load-displacement curve or sudden drops in differential hardness indicated no cracking inside. The film C1 was deposited on hard metal substrate (WC).

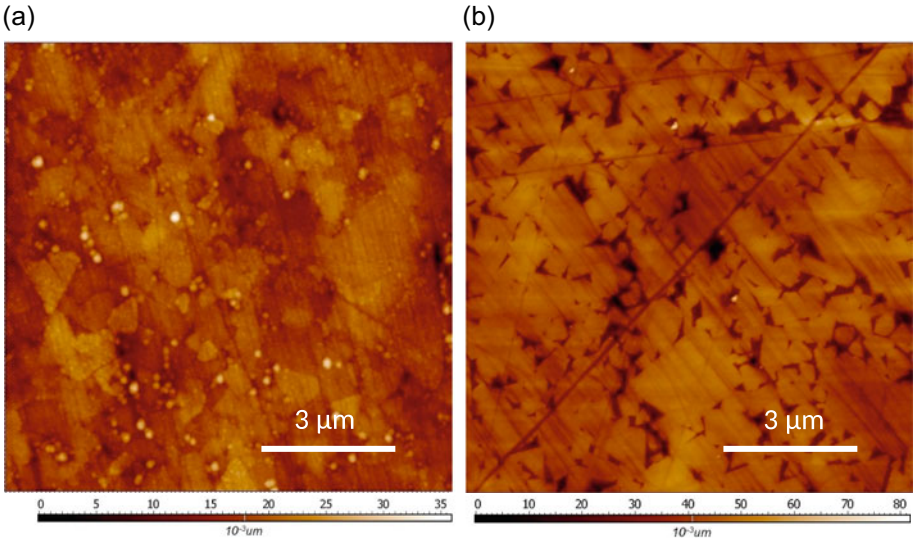

Fig. 7. The AFM images of (a) surface of the sample C2 and (b) uncoated hardmetal substrate.

deformation was controlled by the plastic behaviour of the substrate.

The hardness of amorphous Mo-B-C coatings is comparable with the hardness of most often used amorphous diamond-like carbon coatings [8,13–16]. However, the elastic modulus is significantly higher. Moreover, the crack resistance of the coatings is also substantially enhanced. Even though the maximum indentation depth exceeded the thickness of the coating, only plastic deformation of the coating and the substrate occurred. There were no pop-in events on the loading curve suggesting that no cracks occurred during the indentation (see Fig. 5a). This was also confirmed by the TEM results (see Figs. 2a, 3a and 3b) as well as by depth profiles of differential hardness (see Figs. 5b and 6) where sudden drops indicating cracking were not detected. The sudden differential hardness decrease from indentation depth around 0.25 μm was caused by the expansion of the deformation zone into the softer HSS substrate. The indentation response of the studied sample was fully controlled by plastic deformation of the HSS substrate from indentation depths around 0.5 μm. The hardness and elastic modulus of nanocrystalline Mo-B-C coatings are comparable with common hard coatings used for protective applications [17,18], for example nc-TiC/a-C:H [11,19–24]. However, fracture toughness is generally better for Mo-B-C coatings, especially when compared to nc-TiC/a-C:H that contains more carbon. The nc-TiC/a-C:H coatings with higher titanium content have excellent fracture toughness but, on the other hand, their hardness is generally lower [11,21]. The excellent resistance against brittle failure during tensile testing of Mo_2BC film on copper substrate was also reported [25].

The surface was studied by atomic force microscopy and the results for the nanocrystalline sample C2 are depicted in Figure 7a. The surface of uncoated polished and plasma cleaned hardmetal is in Figure 7b. From Figure 7b it is clear that the uncoated hardmetal contains deeper holes. The peak-to-valley height of hardmetal was 81 nm and the average roughness R_a = 5.1 nm. On the other hand, the calculated peak-to-valley height of the sample C2 was smaller and equaled approximately 36 nm. The average surface roughness of sample C2 was $R_a = 2.1$ nm. The coating obviously filled the holes during its growth and generally smoothed the surface.

4 Conclusion

Magnetron sputtering process was used for the preparation of five Mo-B-C coatings with different microstructures. The correct methodology for hardness and elastic modulus evaluation was developed. Different evolutions of hardness and elastic modulus depending on maximum indentation depth for amorphous and nanocrystalline samples were carried out. This was caused by different inner stress evolution during growth and by different inner structures. The Mo-B-C coating showed very favorable combination of high hardness and elastic modulus together with high fracture toughness. The average hardness of Mo-B-C coatings with amorphous structure was found as 19.5 GPa and their elastic modulus was around 276 GPa. The nanocrystalline Mo-B-C coatings have approximately the same hardness and elastic modulus as the typical nc-TiC/a-C:H coatings. However, the fracture toughness is generally higher for Mo-B-C films. The differential hardness curves and TEM images from the area under the indentation imprint proved that there was no crack formation in the vicinity of the imprints. Also the adhesion after indentation up to 1 N remained sufficient and no delamination occurred. The surface of the samples was studied using AFM. From the presented images and calculated surface roughness it was proven that the Mo-B-C coating smoothed the surface, surface roughness decreased from 5.1 nm for uncoated hardmetal to 2.1 nm.

This research has been supported by the project CZ.1.05/2.1.00/03.0086 funded by European Regional Development

Fund and project LO1411 (NPU I) funded by Ministry of Education Youth and Sports of Czech Republic and The Czech Science Foundation (Project 15-17875S).

References

1. S.F. Pugh, Phil. Mag. **45**, 823 (1954)
2. D.G. Pettifor, Mater. Sci. Technol. **8**, 345 (1992)
3. J. Emmerlich, D. Music, M. Braun, P. Fayek, F. Munnik, J.M. Schneider, J. Phys. D: Appl. Phys. **42**, 185406 (2009)
4. H. Bolvardi, J. Emmerlich, M. to Baben, D. Music, J. von Appen, R. Dronskowski, J.M. Schneider, J. Phys.: Condens. Matter **25**, 045501 (2013)
5. D. Music, J.M. Schneider, JOM **59**, 60 (2007)
6. M.W. Barsoum, T. El-Raghy, Am. Sci. **89**, 334 (2001)
7. H. Bolvardi, J. Emmerlich, S. Mráz, M. Arndt, H. Rudigier, J.M. Schneider, Thin Solid Films **542**, 5 (2013)
8. J. Robertson, Mat. Sci. Eng. R **37**, 129 (2002)
9. W.C. Oliver, G.M. Pharr, J. Mater. Res. **19**, 3 (2004)
10. B. Wolf, Phil. Mag. Phil. Mag. Lett. **86**, 5251 (2006)
11. L. Zábranský, V. Buršíková, J. Daniel, P. Souček, P. Vašina, J. Dugáček, P. St'ahel, O. Caha, J. Buršík, V. Peřina, Surf. Coat. Technol. **267**, 32 (2015)
12. G. Bergerhoff, I.D. Brown, in "*Crystallographic Databases*", edited by F.H. Allen et al. (International Union of Crystallography, Chester, England, 1987)
13. A. Grill, Diam. Relat. Mater. **8**, 428 (1999)
14. D. Franta, V. Buršíková, I. Ohlídal, P. St'ahel, M. Ohlídal, D. Nečas, Diam. Relat. Mater. **16**, 1331 (2007)
15. S. Neuville, A. Matthews, Thin Solid Films **515**, 6619 (2007)
16. S. Neuville, Surf. Coat. Technol. **206**, 703 (2011)
17. A.A. Voevodin et al., in *Nanostructured Thin Films and Nanodispersion Strengthened Coatings*, edited by A.A.Voevodin, D.V. Shtansky, E.A. Levashov, J.J. Moore (NATO Science Series II. Vol. 155, Kluwer Academic Sciences, Dordrecht, 2004)
18. J. Musil, Surf. Coat. Technol. **207**, 50 (2012)
19. A. Czyżniewski, W. Prechtl, J. Mater. Proc. Technol. **157–158**, 274 (2004)
20. P. Souček, T. Schmidtová, L. Zábranský, V. Buršíková, P. Vašina, O. Caha, M. Jílek, A.E. Mel, P.Y. Tessier, J. Schäfer, J. Buršík, V. Peřina, R. Mikšová, Surf. Coat. Technol. **211**, 111 (2012)
21. L. Zábranský, V. Buršíková, P. Souček, P. Vašina, T. Gardelka, P. St'ahel, O. Caha, V. Peřina, J. Buršík, Surf. Coat. Technol. **242**, 62 (2014)
22. Y.T. Pei, D. Galvan, J.Th.M. De Hosson, C. Strondl, J. Eur. Ceram. Soc. **26**, 565 (2006)
23. Y.T. Pei, D. Galvan, J.Th.M. De Hosson, A. Cavaleiro, Surf. Coat. Technol. **198**, 44 (2005)
24. P. Vašina, P. Souček, T. Schmidtová, M. Eliáš, V. Buršíková, M. Jílek, M. Jílek Jr., J. Schäfer, J. Buršík, Surf. Coat. Technol. **205**, s53 (2011)
25. S. Djaziri, S. Gleich, H. Bolvardi, C. Kirchlechner, M. Hans, C. Scheu, J.M. Schneider, G. Dehm, Surf. Coat. Technol. **289**, 213 (2016)